Materials Today Bio 27 (2024) 101142

Contents lists available at ScienceDirect

Materials Today Bio

journal homepage: www.journals.elsevier.com/materials-today-bio

A bioinspired switchable adhesive patch with adhesion and suction mechanisms for laparoscopic surgeries

Xiang Wu [a,b,c,1], Junjie Deng [b,c,d,1], Wei Jian [e,**], Yanyu Yang [b,c,d], Hanjie Shao [a], Xinhua Zhou [a], Ying Xiao [b,c], Jingyun Ma [a], Yang Zhou [a], Rong Wang [b,c,*], Hong Li [a,***]

[a] Ningbo Medical Center Li Huili Hospital, Health Science Center, Ningbo University, Ningbo, 315000, PR China
[b] Laboratory of Advanced Theranostic Materials and Technology, Ningbo Institute of Materials Technology and Engineering, Chinese Academy of Sciences, Ningbo, 315201, PR China
[c] Zhejiang International Scientific and Technological Cooperative Base of Biomedical Materials and Technology, Ningbo Cixi Institute of Biomedical Engineering, Ningbo, 315300, PR China
[d] Wenzhou Medical University, Wenzhou, 325035, PR China
[e] School of Mechanical Engineering & Mechanics, Ningbo University, Ningbo, 315211, PR China

ARTICLE INFO

Keywords:
Hydrogel
Suction cup
Adhesive patch
Biocompatibility
Liver retraction

ABSTRACT

Medical adhesives play an important role in clinical medicine because of their flexibility and convenient operation. However, they are still limited to laparoscopic surgeries, which have demonstrated urgent demand for liver retraction with minimal damage to the human body. Here, inspired by the suction cup structure of octopus, an adhesive patch with excellent mechanical properties, robust and switchable adhesiveness, and biocompatibility is proposed. The adhesive patch is combined by the attachment body mainly made of poly(acrylic acid) grafted with *N*-hydroxysuccinimide ester, crosslinked biodegradable gelatin methacrylate and biodegradable biopolymer gelatin to mimic the adhesive sucker rim, and the temperature-sensitive telescopic layer of microgel-crosslinked poly(*N*-isopropylacrylamide-*co*-2-hydroxyethyl methacrylate) to shrink and form internal cavity with reduced pressure. Through mechanical tests, adhesion evaluation, and biocompatibility analysis, the bioinspired adhesive patch has demonstrated its capacity not only in adhesion to tissues but also in potential treatment for medical applications, especially laparoscopic technology. The bioinspired adhesive patch can break through the limitations of traditional retraction methods, and become an ideal candidate for liver retraction in laparoscopic surgery and related clinical medicine.

1. Introduction

The maturation and widespread adoption of laparoscopic technology have enabled a growing number of abdominal surgeries to be conducted laparoscopically. One of the advantages of laparoscopic surgeries over traditional open abdominal surgeries is that they treat patients with minimal trauma [1]. The laparoscopic technology is flexible for surgical resections by the elevation of the target organ to expose the operative field, especially in the treatment of gastric cancer, liver cancer and pancreatic cancer, which account for over 50 % of cancer-related morbidity and mortality [2,3]. Currently, most patients tend to opt for laparoscopic surgery for treatment. However, the liver is a large organ in the abdomen that is entirely covered by the visceral peritoneum, with the exception of the area in direct contact with the diaphragm, leading to limited maneuverable space and instrument mobility for surgical operation [4]. For complex surgeries such as gastrectomy and pancreaticoduodenectomy, it is often necessary to suspend the liver to fully expose the surgical resection area. Therefore, it is crucial to introduce advanced equipment to achieve optimal liver retraction, but this technical challenge still needs further research. Traditional liver retraction methods by forceful instruments used to suspend the liver not only reduce the space for operation, but also may generate unnecessary

* Corresponding author.
** Corresponding author.
*** Corresponding author.
E-mail addresses: jianwei@nbu.edu.cn (W. Jian), rong.wang@nimte.ac.cn (R. Wang), lihong196311@163.com (H. Li).
[1] X. Wu and J. Deng contributed equally to this work.

https://doi.org/10.1016/j.mtbio.2024.101142
Received 10 April 2024; Received in revised form 7 June 2024; Accepted 28 June 2024
Available online 1 July 2024

injuries to normal tissue by excessive force, causing temporary abnormalities in liver function tests after laparoscopic surgeries. The use of medical adhesives or glues for the attachment with the diaphragm is an effective way to achieve liver suspension [5]. However, most currently commercially available medical adhesives or glues are not developed for laparoscopic surgeries, and have been found to have side effects including contamination, allergic or inflammatory response, toxic degradation, and possibility of compression on surrounding tissues [6]. Therefore, the design and development of suitable adhesive materials for wet tissue surfaces with switchable adhesiveness have become an urgent demand and remain a challenge for laparoscopic surgeries.

Over the past decades, polymer-based adhesives and glues, such as fibrin glues, gelatins, collagens, celluloses, synthesized polymers, and adhesive hydrogels, have been developed for medical applications including regeneration of injured skin, wound dressings, surgical repair, hemostatic sealing, drug delivery, medical implants, and securing biodevices to tissue in wet conditions [7–11]. A variety of different mechanisms, including van der Waals forces, capillary forces, viscous forces, mechanical interlocking, glue through chemical bonding, friction, and suction, can contribute to the adhesion independently or synergistically [12]. Hydrogels show good mechanical properties mainly due to two physical mechanisms: the microscopic kinetic dissociation/association of crosslinks and inelastic conformational changes of gel networks [13], which can be predicted through the combination of theoretical models and experimental measurements [14]. The application of adhesive hydrogels in the field of tissue engineering has also made significant progress [15]. For example, a tough, biocompatible, and bioabsorbable tissue adhesive has been developed for adhesive anastomosis in organ transplantation, which has been successfully applied in a great vein when transplanting the liver of a pig [16]. In addition, the hemostatic microneedle arrays have been developed for rapid blood coagulation by attracting platelets with strong attachment to soft tissues via bioadhesion and interlocking [17]. It is worth noting that a biomimetic adhesive hydrogel inspired by mussels has been successfully applied as bone reinforcement material [18]. However, the existing hydrogels exhibit poor mechanical properties or cannot adhere well to wet surfaces and detach on demand, which makes it difficult to satisfy the needs in biomedical applications, especially in clinical operations with abdominal cavity containing a certain amount of peritoneal fluid.

Achieving strong and switchable adhesion is significant in these material systems, which can be learnt from nature. Remarkable and switchable adhesion performance is commonly found in animals such as geckos, tree frogs, clingfishes, and octopuses [9]. The adhesive organs with special structures enable these animals to attach to different surfaces or capture preys through enhancing the interactive force between animals and target objects, and detach on demand [19]. Especially, the suction cup in an octopus forms strong and switchable adhesion to most surfaces underwater through physical action and internal negative pressure. Synthetic suction cup adhesives have been applied in a variety of applications such as cleaning conveyor systems, soft robotics, wearable devices, and stimulus-responsive adhesives [20–22]. Inspired by the structure of octopus suction cups, a biocompatible wound patch with selective adhesiveness and individualized design has been designed for different skin surfaces [23]. A scalable self-assembly technology for adhesion materials has been proposed to mimic octopus sucker functionality and enables great adhesive capacity on both microrough and flat surfaces in dry and wet environments [24]. Smart adhesive pads inspired by octopus suckers have been developed with excellent switchable adhesion in response to a thermal stimulus [25]. An abalone-inspired sucker integrating an elastic body and a membrane structure is proposed and fabricated filled with rigid quartz particles to adjust the backing stiffness of the contact like abalone [26]. Many other studied have reported various bioinspired hydrogels, such as mussel foot proteins-inspired tissue adhesives with repeatable underwater tissue adhesive hydrogels [27], ctenophores-inspired adhesive hydrogels with fast self-healable capability, reversible underwater adhesion, biocompatibility and antibacterial ability for tissue repair [28], and bioinspired octapeptide hydrogels with concentration-dependent storage modulus and controlled drug-release action for drug encapsulation and delivery [29]. However, adhesive materials are still limited in laparoscopic surgeries that require robust yet switchable adhesion in a wet environment for liver retraction.

In the present work, inspired by the structure of suction cups from octopus, an adhesive patch with high mechanical properties, adjustable adhesive ability, and good biocompatibility is developed for liver retraction in laparoscopic surgeries. The bioinspired adhesive patch, designed to be of an optimal size for effect operation, consists of an attachment body (compose of gelatin-based poly(acrylic acid) hydrogel) to provide adhesion to tissues in wet conditions and a temperature-sensitive telescopic layer (compose of microgel-crosslinked poly(*N*-isopropylacrylamide-*co*-2-hydroxythyl methacrylate) (poly(NIPAM-*co*-HEMA)) in the center of the attachment body to provide strong and switchable adsorption ability, as schemed in Fig. 1. The attachment body provides strong adhesion on the wet surface, while the temperature-sensitive telescopic layer allows for switchable adhesion capability. Demonstrated through mechanical tests, adhesion evaluation, and detailed biocompatibility analysis including *in vitro* hemolysis and cytotoxicity, and *in vivo* implantation, this bioinspired adhesive patch can adhere strongly to tissue surfaces, providing excellent support during organ exposure while minimizing the risk of injury and irritation to tissues, and being detached from the surface on demand. This work presents a novel adhesive patch specifically suitable for liver retraction, and the results indicate that this designed adhesive patch can be a potential and ideal candidate for laparoscopic surgeries that involve tissue and organ retraction.

2. Materials and methods

2.1. Materials

Acrylic acid (AAc, >99 %), gelatin, methyl methacrylate, phosphate-buffered saline (PBS), lithium phenyl-2,4,6-trimethylbenzoylphosphinate (LAP), *N*-isopropyl acrylamide (NIPAM, 98 %), *N*,*N*′-methylenebisacrylamide (MBA, 95 %), potassium persulfate (KPS, AR, 99.5 %), sodium dodecyl sulfate (SDS), 2-hydroxyethyl methacrylate (HEMA), 1-(3-dimethylaminopropyl)-3-ethylcarbodiimide (EDC), 4-dimethylaminopyridine (DMAP), and *N*,*N*,*N*′,*N*′-tetramethylethylenediamine (TEMED, 99 %) were purchased from Aladdin, Shanghai, China. NIH 3T3 cells (GNM 6) were supplied by the Cell Bank of the Chinese Academy of Sciences, Shanghai, China. NIPAM monomers were purified before use, and all other chemicals and solvents used were analytical grade without further purification.

2.2. Preparation of prepolymer solution for the attachment body

The gelatin-based attachment body was prepared through dissolving 30 % (w/w) acrylic acid, 10 % (w/w) gelatin, 1 % (w/w) acrylic acid *N*-hydroxysuccinimide (AAc-NHS) ester, 0.1 % (w/w) gelatin methacrylate (GelMA), and 0.2 % (w/w) LAP in deionized water. The prepolymer solution was then injected into a silicone mold with 5 mm thickness sandwiched between two glass plates using a sterile syringe, and exposed to 365 nm UV light with 15 W power for 20 min to obtain the attachment body of the adhesive patch with a groove with the diameters of 2 cm, 3 cm, and 4 cm and the thicknesses of 2 mm, 3 mm, and 4 mm respectively in the center.

2.3. Synthesis of microgel grafted with vinyl groups

Poly(*N*-isopropylacrylamide) (PNIPAM) microgel (MG) was synthesized by free-radical precipitation polymerization. In particular, 2.848 g of NIPAM, 0.202 g of AAc, and 0.064 g of MBA were dissolved in 200 mL of deionized water, and placed in a round-bottomed three-necked flask

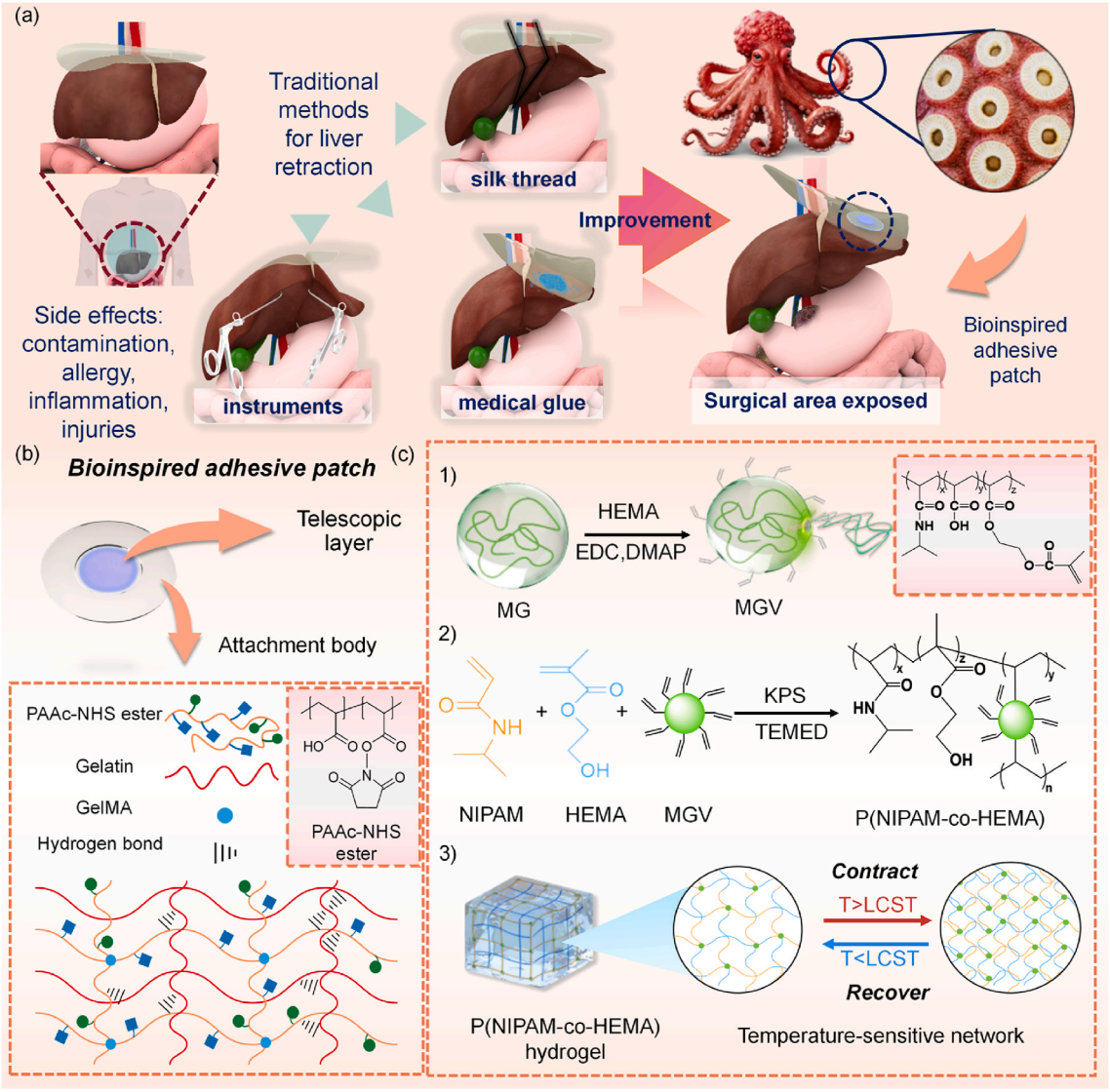

Fig. 1. The design inspiration, strategy, and application prospect of the adhesive patch. (a) Application of traditional methods of liver retraction in laparoscopic surgery and schematic overview of the bioinspired adhesive patch. The components of the bioinspired adhesive patch with synthesis routes of (b) the attachment body and (c) the temperature-sensitive telescopic layer.

fitted with a condenser. The mixture was bubbled with nitrogen for 15 min, and 0.116 g of SDS was then added to the mixture and heated to 70 °C. 0.16 g of KPS dissolved in 4 mL of deionized water was added after 1 h to induce the reaction for 4 h. The synthesized MG was collected and purified via dialysis against deionized water for 3 days. Vinyl groups were grafted onto MG through an esterification reaction with HEMA. 4.78 g of EDC, 3.64 g of HEMA, and 0.17 g of DMAP were added to 100 mL of MG dispersion (containing about 1.5 g microgels), and the reaction mixture was stirred continuously at room temperature for 4 h. The functionalized MG after purification for at least 3 days was lyophilized by freeze-dryer (Scientz-10N multi-manifold common type, Xinzhi Biological Technology, Ningbo, China) and stored at −20 °C to obtain the microgel grafted with vinyl groups (MGV). Proton nuclear magnetic resonance spectra (^{1}H NMR, Ascend 400 MHz Bruker) were recorded with a Varian Mercury plus (400 MHz) spectrometer using deuterated water and deuterated acetic acid as solvent and internal standard to determine chemical structures.

2.4. Fabrication of PNIPAM and poly(NIPAM-co-HEMA) hydrogel

PNIPAM was prepared through a single-pot free radical polymerization. In particular, 3 mol/L (3.4 g) of NIPAM monomers were dissolved in 10 mL of deionized water. For PNIPAM, 0.015 mol/L (0.023 g) of MBA was added as the crosslinking agent at room temperature, and then 0.0015 mol/L (0.0041 g) of KPS was added, followed by nitrogen deoxygenation for 15 min. After incubating in an ice bath for 5 min, TEMED of 20 μL was quickly added and mixed thoroughly. For poly (NIPAM-*co*-HEMA), HMEA was added dropwise with the amounts of 0 mol/L, 0.15 mol/L, 0.30 mol/L, 0.45 mol/L, 0.60 mol/L and 0.75 mol/L respectively and the complete dissolution was achieved. 0.2 g of MGV was added and dispersed completely, followed by the dropwise addition of 0.0015 mol/L (0.0041 g) of KPS. After nitrogen deoxygenation for 15 min and incubation in an ice bath for 5 min, TEMED was quickly added and mixed thoroughly. The obtained mixture was injected into the groove of the suction cup using a syringe until it filled the groove without bubbles. The sample was left for 48 h at room temperature to form the stable poly(NIPAM-*co*-HEMA) hydrogel through free-radical polymerization.

2.5. Shrinkage behavior of poly(NIPAM-co-HEMA)

Poly(NIPAM-*co*-HEMA) hydrogel was cut into samples in a circle

shape with a diameter of 20 mm and a thickness of 2 mm. The shrinkage behaviors of all the hydrogel samples were observed and captured after incubation in deionized water at 37 °C for 1 min, 3 min, and 5 min, and the water retention after shrinkage was measured accordingly. The weight of the dry sample was recorded as W_o, and the weight at each set time point was recorded as W_t. The water retention (W_r) at different time points was recorded through the equation:

$$Wr = (W_t - W_o) / W_o \times 100\%$$

2.6. Thermal properties of poly(NIPAM-co-HEMA) hydrogel

For thermal analysis, the hydrogel was heated from 20 °C to 50 °C, and then cooled from 50 °C to 20 °C in a nitrogen-containing atmosphere at the rate of 10 °C/min. The volume phase transition temperature of hydrogel was determined at the beginning of the endothermic peak during the second heating process using differential scanning calorimetry (DSC, DSC2500, Waters Technology).

2.7. Mechanical tests

The mechanical tests were performed using a universal testing machine (Model C43, MTS standard) with a constant loading rate of 20 mm/min to obtain the tensile properties of poly(NIPAM-*co*-HEMA) hydrogel. The values of stress and strain were calculated based on the average results from four separate measurements.

The adhesion properties of the samples were measured using a universal material testing machine with a 200 N load cell at a speed of 20 mm/min. The diameter and thickness of the attachment and the adhesive patch sample were 50 mm and 5 mm, respectively. For the samples with the thickness ratios of 2:5, 3:5, and 4:5, the values for the thickness of the temperature-sensitive telescopic layers were 2 mm, 3 mm, and 4 mm, and the corresponding values for the diameter were 20 mm, 30 mm, and 40 mm. Porcine skin is selected as the substrate material. For the case at 37 °C, the temperature of the porcine skin was maintained using heated water. The substrate surface of porcine skin was dehaired with excess grease scraped off, rinsed with ethanol, and then with deionized water and dried before use. The adhesion strength was calculated by the measured maximum load divided by the bonded area. Each sample was tested four times, and the average value was used to assess the adhesive properties. The adhesive patch was adhered to the finger of a volunteer to demonstrate the stretchability of the patch. The experiment was conducted with the consent of the volunteer.

2.8. Characterization of microstructure in poly(NIPAM-co-HEMA) hydrogel

For microstructure characterization, the attachment body and poly (NIPAM-*co*-HEMA) were observed by scanning electron microscopy (SEM, Regulus 8230, Hitachi) after removing moisture using a freeze-drying oven (Scientz-10N multi-manifold common type, Xinzhi Biological Technology, Ningbo, China).

2.9. Experimental setup for the removal of the adhesive patch from liver

The trimmed porcine skin was fixed on the surface of the temperature-controlled experimental clamp. One side of the adhesive patch was adhered onto the surface of the porcine skin, and the porcine liver sample was then attached to the other side of the adhesive patch at the temperature of 37 °C. The bonding interface was sprayed with three types of solutions, including pure water, PBS solution, and the mixture of 0.5 mol/L of sodium bicarbonate (SBC) and 50 mmol/L of glutathione (GSH) dissolved in PBS solution. It was found that the detachment of the liver sample from the adhesive patch did not show after the spraying of pure water and PBS solution, while appeared after 10 s with the spraying of the mixture of SBC and GSH in PBS solution.

2.10. Hemolysis assays and cytotoxicity of the adhesive patch

Fresh rabbit blood was filled in an ethylenediaminetetraacetic acid anticoagulation tube, and pipetted into an Eppendorf tube, followed by centrifugation at 1800–2000 rpm at 4 °C for 6–8 min. The serum was extracted into the tube. 0.9 % normal saline with an equal volume was added to the remaining erythrocytes, and it was repeated three times to remove excess serum. The erythrocytes were then suspended in 0.1 M PBS (pH 7.0) and diluted 50-fold (0.5–1 mL of erythrocyte suspension was added to 25–50 mL of PBS) to obtain an erythrocyte suspension with a concentration of 2×10^8 cells/mL. The erythrocyte solution (900 μL) added to the hydrogel immersion fluid (100 μL) was used as the sample group. The erythrocyte suspension (900 μL) added to normal saline (100 μL) and to Triton X-100 (1 %, 100 μL) were used as the negative and positive controls, respectively. After incubation at 37 °C for 60 min, the suspension was centrifuged at 2000 rpm for 8 min at room temperature. The supernatant was added to a 96-well plate, and the absorbance of the supernatant at the wavelength of 541 nm was determined. The hemolysis ratio was calculated using the following formula: Hemolysis ratio (%) = $(A_t - A_{nc})/(A_{pc} - A_{nc}) \times 100$ %, where A_t is the absorbance of the sample group, A_{nc} is the absorbance of the normal saline group, and A_{pc} is the absorbance of the Triton X-100 group.

The *in vitro* cytotoxicity assessment was conducted following the international standard ISO 10993-5. A sample measuring 1 cm × 3 cm × 0.1 cm was immersed in 5.44 mL of Dulbecco's Modified Eagle Medium (DMEM), supplemented with 10 % fetal bovine serum, 10^5 U/L penicillin, and 100 mg/L streptomycin, with a surface area to volume ratio of 1.25 cm^2/mL. The sample was then incubated at 37 °C with 5 % CO_2 for 24 h. Simultaneously, NIH/3T3 fibroblasts were seeded in a 96-well plate at a concentration of 10^4 cells per well. After incubation at 37 °C for 24 h, the cell culture medium was replaced with 100 μL of the sample extract and incubated for an additional 24 h. In the control group, the culture medium was replaced with 100 μL of fresh DMEM. The viability of the cells in each well was assessed using the Cell Counting Kit-8 (CCK-8) assay. For microscopic examination, a 100 μL cell suspension containing a concentration of 10^5 cells/mL was seeded in a confocal culture dish and incubated at 37 °C. After 24 h, the medium was replaced with the same volume of extract as mentioned earlier. The cells were then cultured for an additional 24 h, stained with the Calcein/PI Cell Viability/Cytotoxicity Assay Kit, and observed using confocal laser scanning microscopy (CLSM, TCS SP8, Leica, Germany).

2.11. Animal test model

All animal experiments were approved by the Institutional Animal Ethics Committee of Ningbo University (NBU20220134). The laboratory rabbits (6-8-week housed male New Zealand rabbits, about 2–3 kg) were anesthetized with a 3 % pentobarbital sodium solution, and the abdomen skin was shaved. Their limbs were fixed, and routine disinfection was performed. The blood was taken from the vein at the edge of the ear and sent to the blood routine. The upper abdomen was incised in the middle of the abdomen by a 5 cm incision, and the suction cup was placed between the liver and the septal muscle. The exposure of the hepatic portal was observed after the liver was hung. In the event that no abnormal condition was found, the abdominal muscles and skins of the laboratory rabbits were gradually sutured after the operation, and the wounds were disinfected and bandaged. These rabbits were given a small amount of water 4 h after the operation. After 24 h, the rabbits were anesthetized again, and blood was taken from the vein at the ear margin. Rapid intravenous injection of 10 % potassium chloride at the concentration of 0.5 mL/kg was provided for the execution. The liver and septum muscle specimens were taken out to observe the post-operative reactions, and the liver tissues were taken out for histological analysis.

2.12. Data processing

All the data were expressed as mean standard deviation. Data analysis was performed using IBM SPSS Statistics 26 (IBM Corp., USA) for comparison with one-way ANOVA followed by Tukey's test to indicate statistically significant differences in * ($p < 0.05$), ** ($p < 0.01$), and *** ($p < 0.001$). All tests were repeated at least three times.

3. Results and discussion

3.1. Mechanical properties of the adhesive gelatin-based poly(acrylic acid) attachment body

The attachment body of the bioinspired adhesive patch is mainly made of poly(acrylic acid) grafted with *N*-hydroxysuccinimide ester (PAAc-NHS ester), crosslinked biodegradable GelMA, and biodegradable biopolymer gelatin, and the compositions are based on the previous work of the design of dry double-sided tape [30]. The presence of negatively charged carboxylic acid groups in the PAAc-NHS ester facilitates the rapid hydration and swelling of the attachment body, and consequently, the wet surfaces of various tissues can be dried efficiently within a few seconds under a pressure of around 1 kPa [30]. In addition, these NHS-activated carboxylic acid groups form amide bonds as well as intermolecular bonds including hydrogen bonds and electrostatic interactions with the amino groups on the tissue surfaces simultaneously, which further enhance interfacial adhesion. To evaluate the mechanical performance of the attachment body, mechanical tests including the lap shear test for the shear strength and the tensile test for the tensile strength were performed, as shown in Fig. 2(a) and (b). The attachment body had a high adhesion strength of 66.5 ± 11.5 kPa and a toughness of 108.3 ± 42.1 J/m^2 (Fig. 2(a)). The Young's modulus, tensile strength, and the elongation at break were 66.3 ± 15.7 kPa, 143.1 ± 35.7 kPa, and 1365.4 ± 266.7 %, respectively (Fig. 2(b)). The results show that the attachment body presents good mechanical properties, which are attributed to the strong hydrogen bonding, electrostatic interactions, and covalent bonds at the interface. The gelatin acts as the bridging polymer between the tissue and the adhesive patch and provides robust adhesion to the tissues. The adhesive patch can withstand a load of 1 kg at least (see Fig. 2(c)). In consideration of practical applications in laparoscopic surgeries, the adhesion performance on the porcine liver sample was evaluated, and it was found that it strongly stuck to the liver tissue (approximately of 1 kg) even after water flushing (see Fig. 2(d)), indicating robust adhesiveness with the tissues for liver retraction. The adhesive was also attached to the human finger to evaluate its bending performance. It was observed in Fig. 2(e) that the attachment body can withstand large bending with an angle of 90°. The excellent bending performance may be attributed to the dissociation of the hydrogen bonds and macromolecular chain slippage caused by external forces [31].

3.2. Thermal-mechanical properties of the temperature-sensitive telescopic layer

Poly(NIPAM-*co*-AAc) microgels were synthesized using precipitation polymerization of NIPAM and AAc, and grafted with vinyl groups by esterifying with HEMA according to our previous study (Fig. 3(a)) [32]. The successful introduction of vinyl groups on poly(NIPAM-*co*-AAc) microgel was confirmed by the appearance of new peaks at 6.15 and 5.77 ppm in the ^{1}H NMR spectrum (Fig. 3(b)). The new peak at 4.22 ppm (protons in -*O*–CH_2–CH_2-*O*-) further confirmed the successful grafting of HEMA to the microgels. About 23 % of the carboxyl groups in the microgel reacted with HEMA as calculated from the ratio of the integration area of the peak of protons in the vinyl groups to those in CH $(CH_3)_2$ in NIPAM units (3.91 ppm). The low critical solution

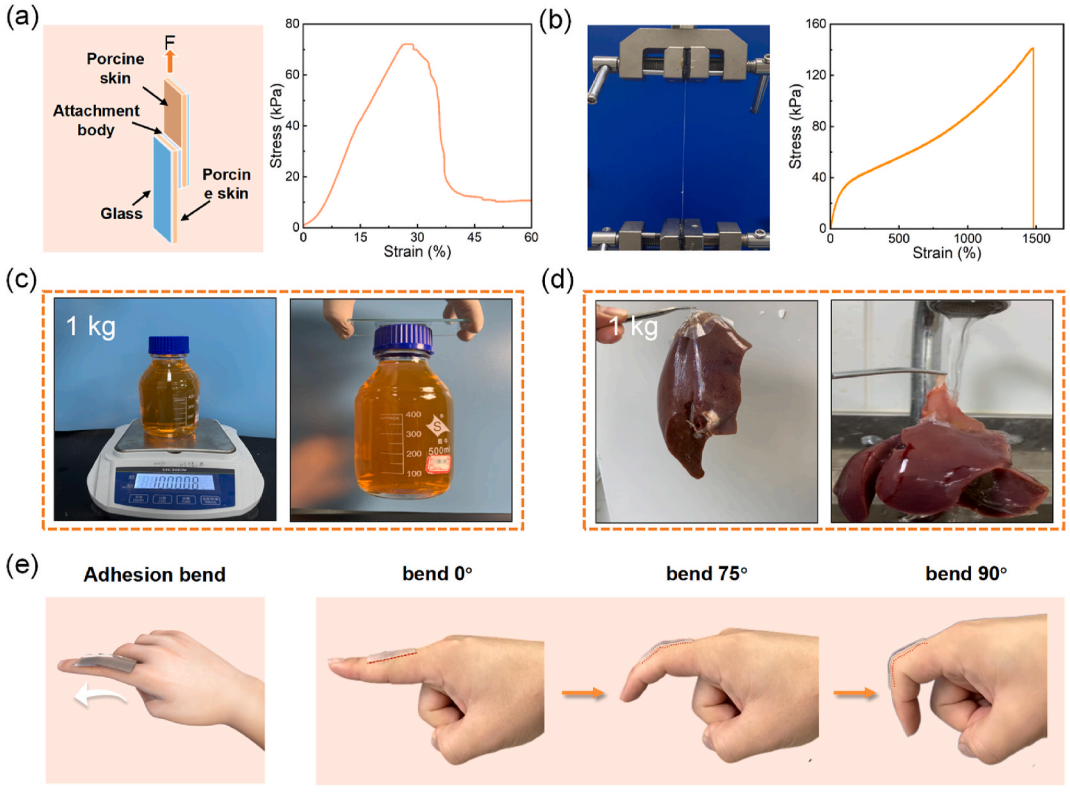

Fig. 2. Mechanical and adhesion properties of the attachment body at room temperature. (a) Lap shear test of the attachment body to porcine skin and the corresponding stress-strain curve. (b) Tensile test of the attachment body and the corresponding stress-strain curve. (c) Adhesion ability of the attachment body between the glass and the bottle with a weight of 1 kg. (d) The adhesion test with the 1 kg porcine liver sample. (e) The demonstration of the bending behavior of the adhesive patch adhering on human finger.

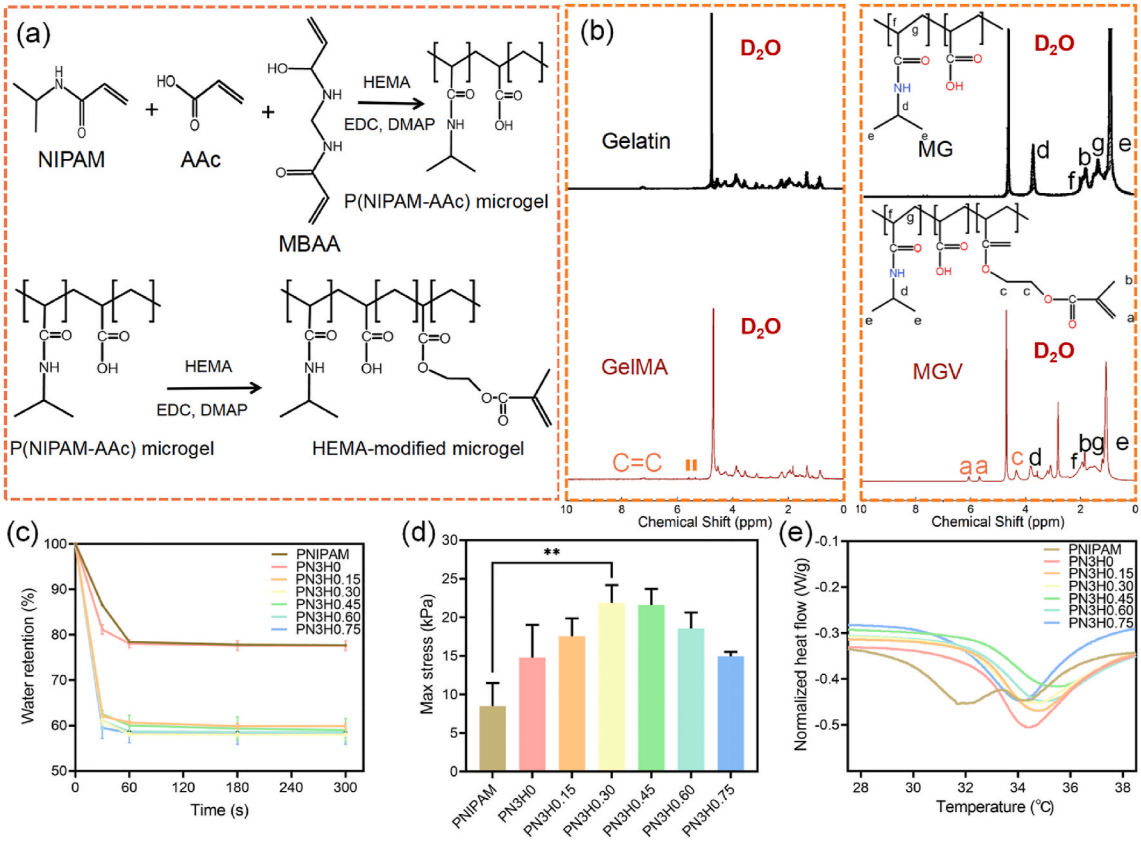

Fig. 3. Synthesis formulas for (a) P(NIPAm-*co*-AAc) microgel and HEMA-modified microgel respectively, and ^{1}H NMR spectra of (b) gelatine, GelMA, MG, and MGV, respectively. The corresponding characterization of thermal-mechanical properties in PNIPAM and poly(NIPAM-*co*-HEMA) samples: (c) Water retention over 5 min at 37 °C. (d) Tensile strength of PNIPAM hydrogel and poly(NIPAM-*co*-HEMA) hydrogels with various amounts of HEMA. (e) DSC curves of PNIPAM hydrogel and poly (NIPAM-*co*-HEMA) hydrogels with various amounts of HEMA.

temperature (LCST) of vinyl-functionalized microgels (MGV) was determined to be 46.9 °C and they were used for fabrication of thermo-responsive poly(NIPAM-*co*-HEMA) consisting of PNIPAM and poly(2-hydroxyethyl methacrylate) (PHEMA), which was applied as the temperature-sensitive telescopic layer. Thermo-responsive property is an important factor for the temperature-sensitive telescopic layer, which exhibits discontinuous changes in their conformations or physical properties at a LCST [32–34]. The layer can swell with water absorption or shrink with dehydration at the temperature around LCST, resulting in a significant change in volume (see Fig. 1(c)). The hydration and dehydration of PNIPAM polymer chains cause the phase transition of PNIPAM in water, and the polymer chains are dehydrated due to the activation of movement of water molecules at temperature levels higher than LCST [35]. Furthermore, PHEMA has good mechanical properties as well as long-term biocompatibility and stability. As a result, the copolymer with the combination of PNIPAM and PHEMA inherits these advantageous characteristics. PNIPAM-based hydrogel has been used in human clinical studies for tissue regeneration [36]. The effects of the crosslinking agent and the amount of HEMA addition on the thermo-mechanical properties of the temperature-sensitive telescopic layer are investigated. MBA and MGV were used as crosslinking agents. The concentration of NIPAM was set at 3 mol/L with the amounts of HEMA selected at 0 mol/L, 0.15 mol/L, 0.30 mol/L, 0.45 mol/L, 0.60 mol/L, and 0.75 mol/L for the preparation of hydrogels of PN3H0, PN3H0.15, PN3H0.30, PN3H0.45, PN3H0.60, and PN3H0.75, respectively. The shrinkage behavior in drainage of the temperature-sensitive telescopic layer is evaluated at 37 °C for up to 5 min. As illustrated in Fig. 3(c), when PNIPAM was synthesized using only MBA or MGV as a crosslinker, it exhibited a shrinkage of approximately 20 % after heating to 37 °C for 5 min. In contrast, the poly(NIPAM-*co*-HEMA) crosslinked by MGV exhibited a shrinkage of approximately 40 % after 5 min. This phenomenon may be attributed to the increased hydrophilicity due to the hydroxyl group in HEMA. When the hydrogel was placed at a temperature exceeding the LCST, it released a higher content of water, resulting in a correspondingly larger shape change, as illustrated in Fig. S1. This indicates a stronger temperature-sensitive response in the poly(NIPAM-*co*-HEMA) crosslinked by MGV. The maximum tensile stress in each case was measured in Fig. 3(d). The tensile strength of MBA-crosslinked PNIPAM hydrogel was 8.5 ± 3.0 kPa, and it increased to 14.8 ± 4.2 kPa for the MGV-crosslinked PNIPAM hydrogel. After copolymerization with HEMA, the tensile strength of the hydrogel further increased, with the maximum tensile strength was achieved with a value of 21.9 ± 2.3 kPa for poly(NIPAM-*co*-HEMA) with 0.30 mol/L HEMA and crosslinked by MGV. This is probably because of the formation of hydrogen bonding by the hydroxyl group in HEMA, thereby increasing the strength of the hydrogel. The mechanical strength of the MGV-crosslinked poly(NIPAM-*co*-HEMA) hydrogel then decreased as the HEMA content further increased from 0.45 mol/L to 0.75 mol/L, probably due to the excessive or uneven distribution of the crosslinking points. The high mechanical property of the poly(NIPAM-*co*-HEMA) hydrogel is important to ensure the integrity and functionality of the telescopic layer of the patch. The LCST phase transition of the poly (NIPAM-*co*-HEMA) hydrogel with various copolymer ratios was measured through DSC as shown in Fig. 3(e). The LCST of the PNIPAM crosslinked by MBA is about 31.9 °C, while that of the PNIPAM crosslinked by MGV (*i.e.,* PN3H0) and poly(NIPAM-*co*-HEMA) crosslinked by MGV with the addition of HEMA (*i.e.,* PN3H0.15, PN3H0.30, PN3H0.45, PN3H0.60, and PN3H0.75) is about 34.1 °C. This indicates that MGV crosslinking increased the LCST of telescopic layer, and copolymerization of HEMA did not affect the LCST significantly. The increase in the

LCST of the MGV-crosslinked hydrogels is likely due to the formation of additional hydrogen bonding by the carboxyl groups with water in MGV [32]. The LCST of MGV-crosslinked poly(NIPAM-*co*-HEMA) is closer to the normal body temperature, which satisfies the condition in human body for temperature sensitivity. When the temperature exceeds LCST, PNIPAM transforms from linear micelles to spherical ones, and the hydrophobic portion inside the micelles shrinks inward, resulting in smaller gel volume and smaller gel mesh, and its temperature sensitivity refers to the above transformation properties. The LCST phase transition with an endothermic process was clearly observed for all the samples, and the exhibited endothermic peaks were attributed to the dehydration of the polymer chains [37]. The PNIPAM crosslinked by MBA shows the largest endothermic peaks. The poly(NIPAM-*co*-HEMA) with smaller amount of HEMA shows smaller peaks, which is attributed to the smaller number of NIPAM units being involved in dehydration upon heating [38]. Such a phenomenon has been observed in the previous study with relatively low enthalpy change [39].

3.3. Characterization and adhesion performance of the adhesive patch

The bioinspired adhesive patch designed in this study is expected to display excellent adhesiveness to human tissue during surgeries. Since porcine skin is similar to human skin tissues in terms of mechanical toughness, it was chosen as the model to evaluate the adhesion property of the adhesive patch. The assembly of the adhesive patch was through injecting the prepolymerization solution of the temperature-sensitive layer into the grooves of the attachment body in an ice bath, and the reaction was continued for 48 h to make it bonded to the attachment body (see Fig. 4(a)). Since the adhesive patch is a combination of two components, the connection between these two materials is analyzed using SEM. The microstructures of the attachment body (see Fig. 4(b1)-4(b3)), the temperature-sensitive telescopic layer (see Fig. 4(c1)-4(c3)), and the junction part between the attachment body and the thermosensitive telescopic layer (see Fig. 4(d1)-4(d3)) were observed under SEM. The joint site shows the strong bonding between the attachment body and the thermosensitive telescopic layer. Furthermore, incubation of the adhesive patch for up to 24 h caused enlargement of the pores in the telescopic layer, but did not damage the bonding of the attachment body to the telescopic layer (Fig. S3), indicating the good stability of the adhesive patch.

To achieve the optimal performance of the adhesive patch, the mechanical tests with the setup shown in Fig. 5(a) were performed with different diameter ratios and thickness ratios between the attachment body and the temperature-sensitive telescopic layer under room temperature and the normal body temperature, *i.e.*, 37 °C. Pulling directly the liver sample fixed in experimental apparatus using the adhesive patch can easily cause tearing due to the fragile nature of the liver. In this case, porcine skin is applied for the experiment. In Fig. 5(b) and (c), it was observed that the adhesion properties exhibit minimal change at room temperature, but significant differences at normal body temperature. At 37 °C, the adhesive design with a diameter ratio of 3:5 (cm, telescopic layer: attachment body) and thickness ratio of 2:5 (mm, telescopic layer: attachment body) demonstrated the highest adhesive strength, reaching 11.5 ± 1.3 kPa. This may be attributed to the increased thickness of the temperature-sensitive telescopic layer, leading to dehydration of the system at its critical temperature and resulting

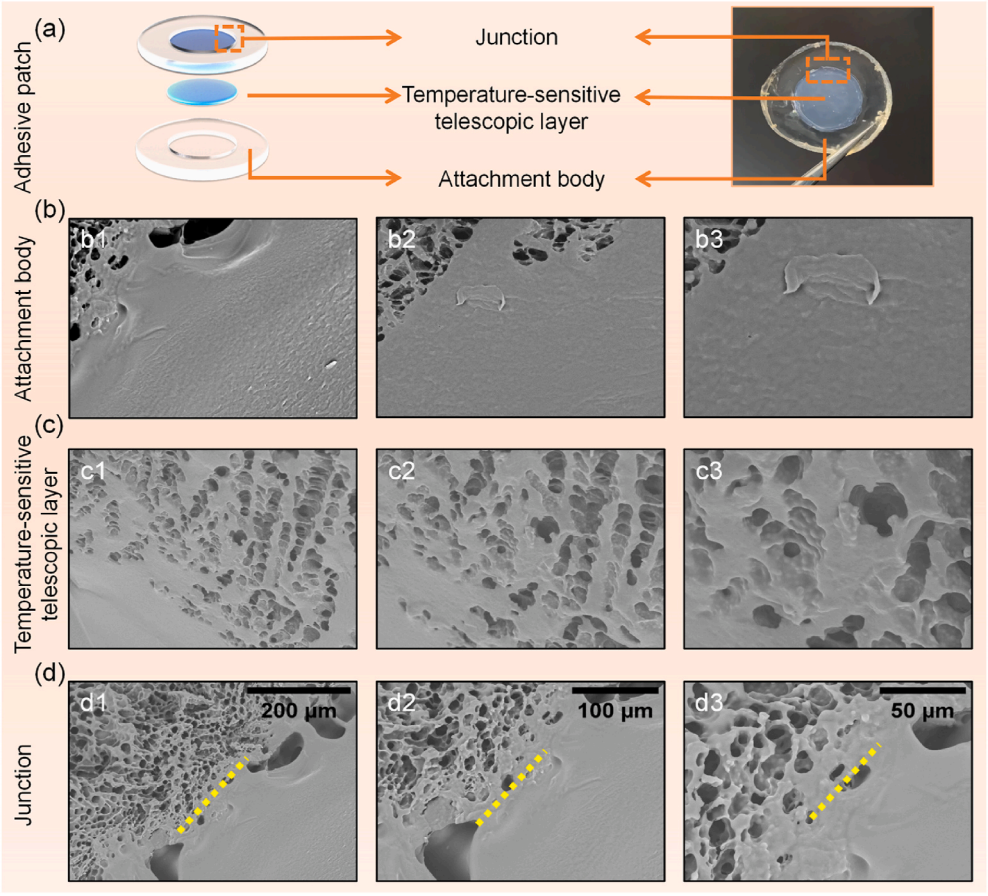

Fig. 4. (a) The structure of the adhesive patch. The SEM images of (b) the attachment body with solid structure, (c) the temperature-sensitive telescopic layer with porous structures, and (d) the junction part of the interface between the adhesive patch and the temperature-sensitive telescopic layer showing tight bonding. The yellow dashed lines in (d1)-(d3) highlight the interface between the attachment body and the temperature-sensitive telescopic layer. (For interpretation of the references to colour in this figure legend, the reader is referred to the Web version of this article.)

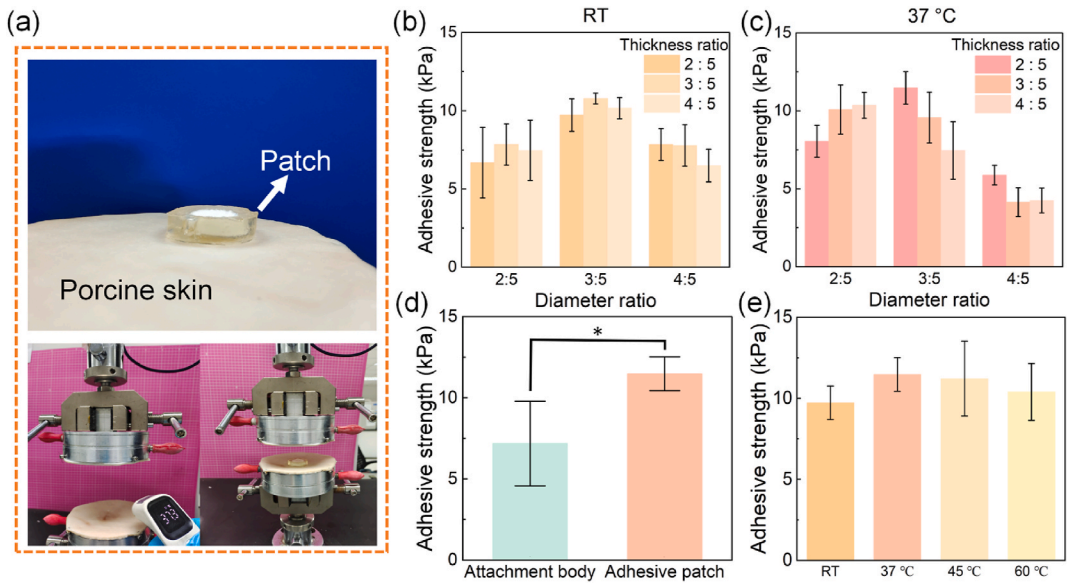

Fig. 5. (a) The experimental setup of tensile tests of the adhesive patch on the porcine skin. The adhesive strength of the adhesive patch with various thickness and diameter ratios was measured at (b) room temperature and (c) 37 °C. (d) The adhesive strength of the attachment body and the adhesive patch at 37 °C. (e) The variation in adhesive strength of adhesive patches with a diameter ratio of 3:5 (cm) and a thickness ratio of 2:5 (mm) at different temperatures. * represents $p < 0.05$.

in an accumulation of water at the bonding interface, thereby affecting internal negative pressure and reducing bonding strength. This effect is negligible at room temperature. As shown in Fig. 5(d), the adhesion strength of adhesive patches with a diameter ratio of 3:5 (cm) and a thickness ratio of 2:5 (mm) was tested at 37 °C, and it was found that the adhesive strength of the adhesive patches was superior to that of the attachment body with the same size. Furthermore, the adhesive strength of adhesive patches with a diameter ratio of 3:5 (cm) and a thickness ratio of 2:5 (mm) at different temperatures was also investigated (see Fig. 5(e)). The results demonstrated that there was no significant difference in the mechanical changes when the temperature exceeded the LCST.

These results indicate that the adhesive patch with the optimal diameter ration of 3:5 (cm) and thickness ratio of 2:5 (mm) can provide robust adhesive and suction functions as well as switchable adhesive ability for liver retraction in clinical applications. In addition, the adhesive patch can be removed easily by spraying to the interface with the mixture of SBC and GSH dissolved in PBS solution, which has been tested on porcine liver sample (see Fig. 6, and Video S1, S2, and S3 in Supplementary Materials). Specifically, SBC in the solution could cleave physical crosslinking (*i.e.,* hydrogen bonding, electrostatic interactions) between the attachment body and the tissue surface through neutralization of the carboxyl groups [40]. GSH has been demonstrated to possess free radical scavenging properties and reduces the potential damage to liver tissue caused by sucker adhesion [41].

3.4. Mechanisms of switchable adhesion and suction

The robust adhesion and suction functions to tissues come from the two components of the adhesive patch. The attachment body is designed to quickly adhere to wet tissues when applied, forming strong bonding. Additionally, a large number of carboxylic acid groups in the polyacrylic acid-based networks can immediately form intermolecular bonds, specifically hydrogen bonds, and electrostatic interactions with the surface of the tissues [42]. Moreover, the attachment body is equipped with cleavable NHS ester groups that are grafted to the PAA network. These ester groups create stable covalent bonds, specifically amide bonds, with the primary amine groups that are abundant on the surface of the tissues [42], as illustrated in Fig. 7(a). This combination of physical and chemical interactions ensures an instant and reliable connection between the attachment body and the wet tissues.

In addition, the temperature-sensitive telescopic layer provides the suction function during application. The temperature-sensitive telescopic layer remains flat with neutral pressure at the room temperature (see Fig. 7(b)). When the temperature exceeds LCST, it shrinks to a reversible conformation due to the hydrogen bond interactions and the hydrophobic effect, and the corresponding structure transforms into similar shape of octopus's sucker. The attachment body contracts due to the strong bonding with the telescopic layer, and the volume of the telescopic layer is formed at the interface with the tissue as shown in Fig. 7(b). During this process, the attachment body adheres firmly to the tissue, thereby forming a closed internal cavity with decreased pressure due to the shrinkage of the thermo-responsive telescopic layer. Such a pressure difference through the suction cup structure leads to the increase in the adhesion strength [21]. As shown from the experiments in the previous section, the removal of the adhesive patch can be realized through treatment of SBC and GSH mixture due to the cleavage of the physical crosslinking structures at the adherent-tissue interface.

3.5. Biocompatibility testing for the adhesive patch

The adhesive patch is in direct contact with the liver and probably blood in laparoscopic surgeries, and therefore it is required to have good hemocompatibility and cell compatibility and does not cause damage to cells. The effect of materials in the adhesive patch on blood and mammalian cells were examined through hemolysis assays and CCK-8. The results show in Fig. 8(a) that similar to the situation in normal saline, the adhesive patch does not cause hemolysis. Fig. 8(b) demonstrates that the calculated hemolysis ratios are less than 5 %, which is the acceptable limit of a hemocompatible material, indicating that it does not affect the internal environmental homeostasis of tissues. The LIVE/DEAD staining results in Fig. 8(c) and the CCK-8 detection results in Fig. 8(d) show that the cells cultured with the control and sample groups exhibit comparable viability, and their growth trends are similar over time from Day 1 to Day 3 as the optical density (OD) values between the control group and the sample group vary slightly, suggesting that the adhesive patch with certain cell proliferation effects has no cytotoxicity and does not cause apoptosis. Since the adhesive patch is used for liver retraction and subsequently removed after operation, the biodegradability after suturing is not considered in this study.

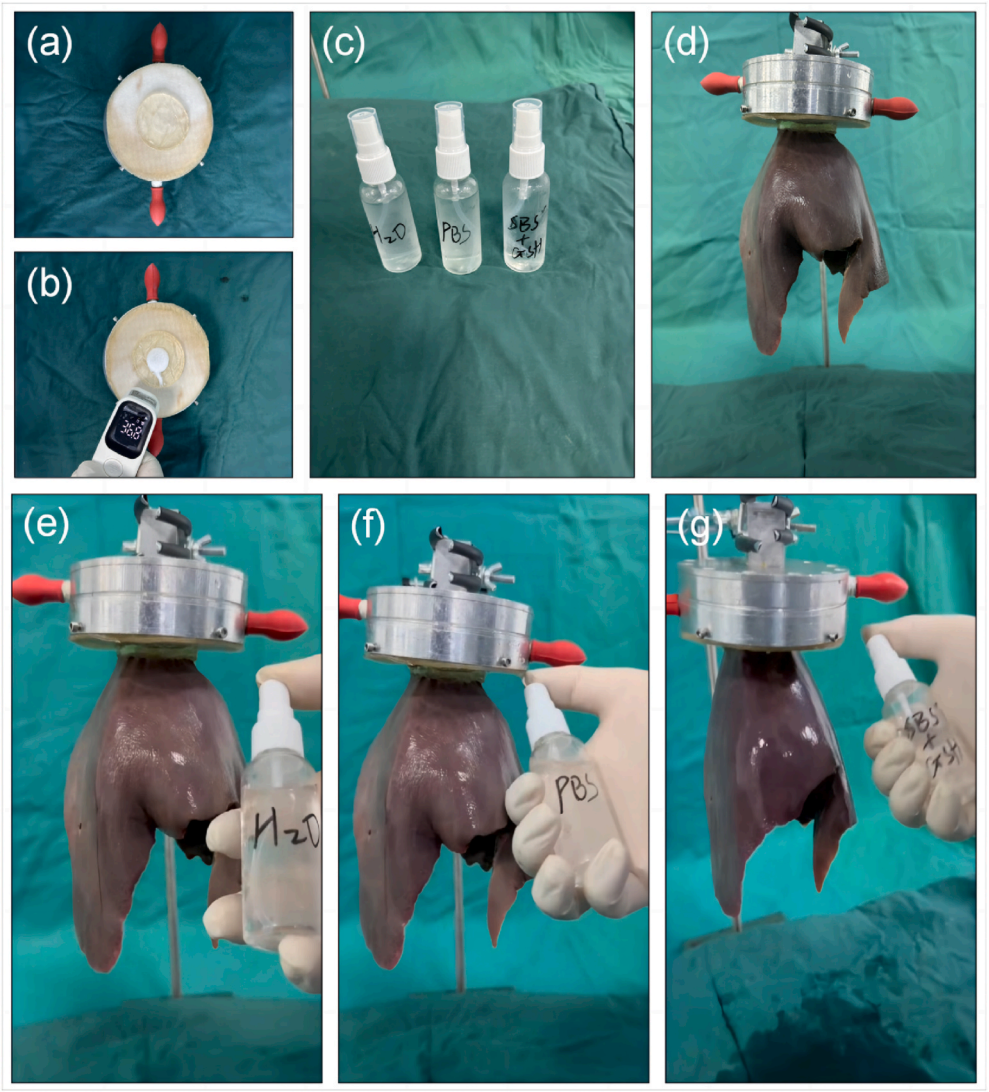

Fig. 6. The setup for the removal of the adhesive patch from liver: (a) the bonding of adhesive patch to the experimental clamp at room temperature; (b) the bonding of adhesive patch to the experimental clamp at the temperature of 37 °C; (c) the three applied solutions including pure water, PBS solution, and the mixture of SBC and GSH dissolved in PBS solution; (d) the bonding of the liver tissue to the adhesive patch; the spraying of (e) water, (f) PBS, and (g) SBC + GSH solutions to the bonding interface.

3.6. *In vivo animal study on rabbits*

The inflammation and infection after the treatment with medical facilities are a major concern for clinical medicine, and therefore the *in vivo* biocompatibility properties of the adhesive patch have been evaluated by the adhesion to the liver surface in laboratory rabbits for 24 h (see Fig. 9(a)). Hematoxylin and eosin (H&E) staining was also carried out to investigate the reaction of the tissue after treatment. The results before and after the treatment with the adhesive patch shown by the images in Fig. 9(b) and (c) demonstrated that only a few erythrocyte deposits were observed in liver tissue after 24 h of implantation, and there was no significant inflammatory reaction found in the sample group. In addition, the counts of inflammatory cells including white blood cells (Fig. 9(d)) and neutrophil granulocytes (Fig. 9(e)) were accessed in both preoperative and postoperative cases. The quantitative analysis results between the preoperative and postoperative groups in six laboratory rabbits show that the number of white blood cells was indifferent. The number of neutrophil granulocytes increased in the postoperative case probably due to the surgically induced stress response in laboratory rabbits, but they all were within the normal limits with complete adherence to aseptic procedures. There was no obvious tissue damage, lesions, inflammation, or noticeable abnormality observed in the major organs of all the laboratory rabbits, indicating that the designed adhesive patch is biocompatible to normal tissues.

4. Conclusions

With the vigorous exploration of animals and biomaterials in wet environments, bioinspired hydrogel has evolved to meet the versatile needs of medical applications. An adhesive patch inspired by the suction cup structure in octopus has been successfully fabricated in this study. The bioinspired adhesive patch consisting of the attachment body and the temperature-sensitive telescopic layer showed excellent mechanical properties and robust and on-demand adhesive performance through tensile and adhesion tests and thermal analysis, which ensure strong and switchable tissue adhesion. The adequate biocompatibility with non-toxicity to the living tissue intraoperatively was further demonstrated through hemolysis, cytotoxicity analysis, and *in vivo* animal experiments. The favorable properties of the bioinspired adhesive patch including high elasticity, mechanical strength, and stability demonstrate the desirable potential for liver retraction during laparoscopic surgeries, and it has overcome the limitations in traditional methods for

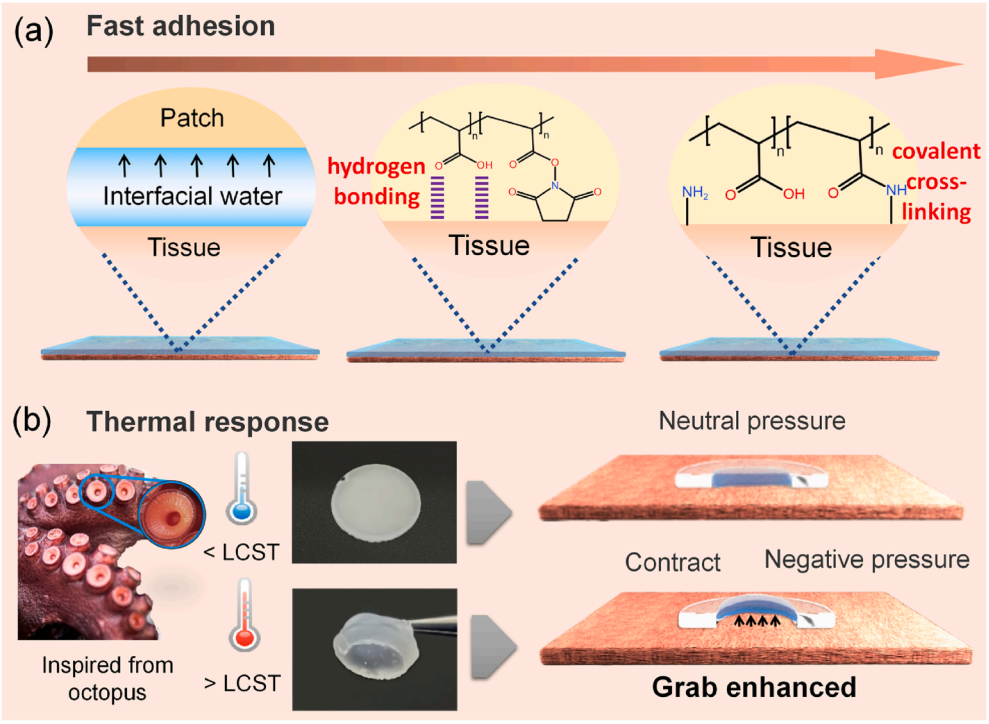

Fig. 7. Schematic illustration of the adhesion and suction mechanisms of (a) the attachment body and (b) the temperature-sensitive telescopic layer.

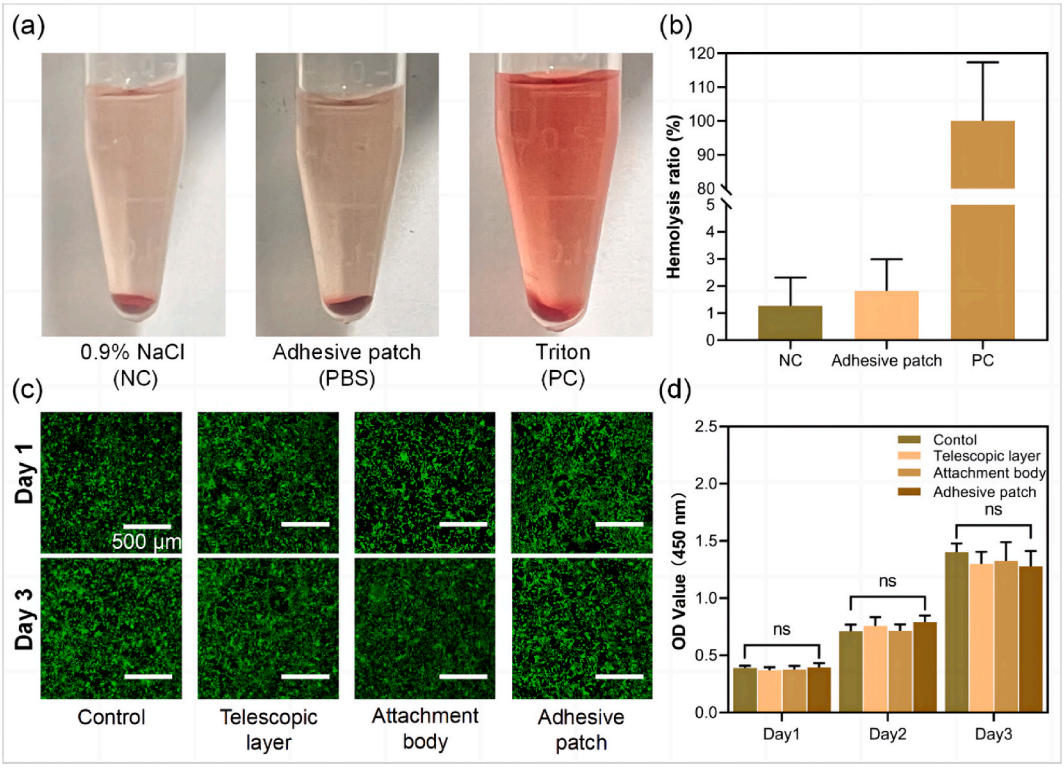

Fig. 8. Hemolysis and cytotoxicity of the bioinspired adhesive patch. (a) Hemolysis performance of the prepared sample in normal saline, adhesive patch with saline, and 1 % Triton X-100, respectively. The results show that the adhesive patch has similar hemolysis with normal saline. (b) The corresponding hemolysis ratios of the negative control (NC) group, the adhesive patch, and the positive control (PC) group. (c) LIVE/DEAD staining of NIH-3T3 cells in both the control group and the sample group extracted for 24 h and 72 h culture. Green fluorescence represents viable cells. (d) The OD value of the control and sample groups by the CCK-8 assay after 1, 2, and 3 days. Ns means no significance. (For interpretation of the references to colour in this figure legend, the reader is referred to the Web version of this article.)

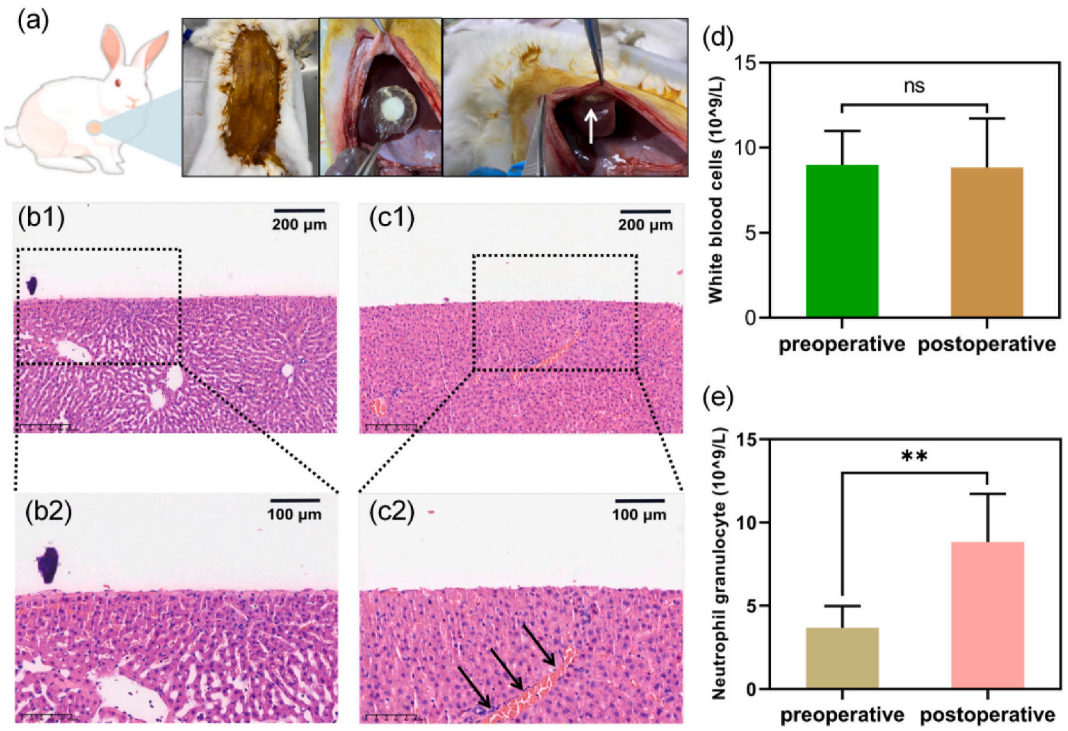

Fig. 9. *In vivo* study of adhesive patch applications. (a) Implantation of adhesive patch on the liver in the laboratory rabbit for 24 h, and the white arrow indicates the position of the adhesive patch. H&E staining of the implantation region of the liver tissue in (b1)(b2) the preoperative and (c1)(c2) postoperative cases with visible erythrocyte precipitation (black arrows). Numbers of (d) white blood cells and (e) neutrophil granulocytes before and after treatment for 24 h. In statistical analysis, a p-value <0.05 is considered statistically significant. In this case, ns means no significance, and ** represents $p < 0.01$.

laparoscopic surgeries, which not only promotes the development of the state-of-the-art adhesive technology, but also provides more flexibility for clinical medicine.

CRediT authorship contribution statement

Xiang Wu: Writing – original draft, Methodology, Investigation, Funding acquisition, Formal analysis, Data curation, Conceptualization. **Junjie Deng:** Methodology, Formal analysis, Data curation. **Wei Jian:** Writing – review & editing, Supervision, Investigation, Formal analysis. **Yanyu Yang:** Investigation, Data curation. **Hanjie Shao:** Methodology, Investigation. **Xinhua Zhou:** Investigation. **Ying Xiao:** Investigation. **Jingyun Ma:** Investigation. **Yang Zhou:** Investigation. **Rong Wang:** Writing – review & editing, Supervision, Resources, Project administration, Methodology, Funding acquisition, Conceptualization. **Hong Li:** Supervision, Resources, Investigation, Funding acquisition.

Declaration of competing interest

The authors declare that they have no known competing financial interests or personal relationships that could have appeared to influence the work reported in this paper.

Data availability

Data will be made available on request.

Acknowledgements

This study was supported by Ningbo Public Welfare Science and Technology Program (2021S106), Youth Innovation Promotion Association CAS (2021296), SRIP Research Project Fund of Ningbo University (2023SRIP1921, 2023SRIP1940), Research and Innovation Foundation of Ningbo University (IF2023059), Key Research and Development Program of Ningbo (2022Z132), and General Surgery Clinical Key Specialty Construction Project of Zhejiang Province (No.2023-SZZ).

Appendix A. Supplementary data

Supplementary data to this article can be found online at https://doi.org/10.1016/j.mtbio.2024.101142.

References

[1] K. Søreide, B. Skjold-Ødegaard, K. Thorsen, H. Kørner, Adhesions after open and laparoscopic abdominal surgery, The Lancet 397 (2021) 95–96, https://doi.org/10.1016/S0140-6736(20)32409-0.
[2] E. Lin, R. Gonzalez, K.R. Venkatesh, S.G. Mattar, S.P. Bowers, K.M. Fugate, T. G. Heffron, C.D. Smith, Can current technology be integrated to facilitate laparoscopic living donor hepatectomy? Surg. Endosc. 17 (5) (2003) 750–753, https://doi.org/10.1007/s00464-002-8858-y.
[3] H. Sung, J. Ferlay, R.L. Siegel, M. Laversanne, I. Soerjomataram, A. Jemal, F. Bray, Global Cancer Statistics 2020: GLOBOCAN Estimates of Incidence and Mortality Worldwide for 36 Cancers in 185 Countries, CA. Cancer J. Clin. 71 (2021) 209–249, https://doi.org/10.3322/caac.21660.
[4] H. Vernon, C.J. Wehrle, V.S.K. Alia, A. Kasi, Anatomy, Abdomen and Pelvis: Liver, StatPearls Publishing, Treasure Island (FL), 2022.
[5] S. Wu, H. Yu, Y. Fan, J. Kong, X. Yu, Liver retraction using n-butyl-2-cyanoacrylate glue during single-incision laparoscopic upper abdominal surgery, Brit. J. Surg. 101 (2014) 546–549, https://doi.org/10.1002/bjs.9446.
[6] G.M. Taboada, K. Yang, M.J.N. Pereira, S.S. Liu, Y. Hu, J.M. Karp, N. Artzi, Y. Lee, Overcoming the translational barriers of tissue adhesives, Nat. Rev. Mater. 5 (2020) 310–329, https://doi.org/10.1038/s41578-019-0171-7.
[7] Y. Chen, J. Meng, Z. Gu, X. Wan, L. Jiang, S. Wang, Bioinspired multiscale wet adhesive surfaces: structures and controlled adhesion, Adv. Funct. Mater. 30 (2020) 1905287, https://doi.org/10.1002/adfm.201905287.
[8] C. Cui, W. Liu, Recent advances in wet adhesives: Adhesion mechanism, design principle and applications, Prog. Polym. Sci. 116 (2021) 101388, https://doi.org/10.1016/j.progpolymsci.2021.101388.
[9] H. Fan, J.P. Gong, Bioinspired underwater adhesives, Adv. Mater. 33 (2021) 2102983, https://doi.org/10.1002/adma.202102983.
[10] T.M. Lutz, C. Kimna, A. Casini, O. Lieleg, Bio-based and bio-inspired adhesives from animals and plants for biomedical applications, Mater. Today Bio. 13 (2022) 100203, https://doi.org/10.1016/j.mtbio.2022.100203.
[11] Y. Lv, F. Cai, Y. He, L. Li, Y. Huang, J. Yang, Y. Zheng, X. Shi, Multi-crosslinked hydrogels with strong wet adhesion, self-healing, antibacterial property, reactive

oxygen species scavenging activity, and on-demand removability for seawater-immersed wound healing, Acta Biomater 159 (2023) 95–110, https://doi.org/10.1016/j.actbio.2023.01.045.
[12] W. Li, Y. Zheng, W. Pang, P. Lai, Bio-inspired adhesive hydrogel for wound healing, Biomed. Tech 1 (2023) 65–72, https://doi.org/10.1016/j.bmt.2022.11.009.
[13] V. Nele, J.P. Wojciechowski, J.P.K. Armstrong, M.M. Stevens, Tailoring gelation mechanisms for advanced hydrogel applications, Adv. Funct. Mater. 30 (2020) 2002759, https://doi.org/10.1002/adfm.202002759.
[14] J. Lin, H. Li, F. Zhu, Q. Ge, J. Qian, R. Xiao, Network alteration of cyclically loaded elastomers mediated by dynamic bonds, J. Mech. Phys. Solids. 179 (2023) 105400, https://doi.org/10.1016/j.jmps.2023.105400.
[15] Y. Zhao, S. Song, X. Ren, J. Zhang, Q. Lin, Y. Zhao, Supramolecular adhesive hydrogels for tissue engineering applications, Chem. Rev. 122 (2022) 5604–5640, https://doi.org/10.1021/acs.chemrev.1c00815.
[16] K. Liu, H. Yang, G. Huang, A. Shi, Q. Lu, S. Wang, W. Qiao, H. Wang, M. Ke, H. Ding, T. Li, Y. Zhang, J. Yu, B. Ren, R. Wang, K. Wang, H. Feng, Z. Suo, J. Tang, Y. Lv, Adhesive anastomosis for organ transplantation, Bioact. Mater. 13 (2022) 260–268, https://doi.org/10.1016/j.bioactmat.2021.11.003.
[17] R. Haghniaz, H.J. Kim, H. Montazerian, A. Baidya, M. Tavafoghi, Y. Chen, Y. Zhu, S. Karamikamkar, A. Sheikhi, A. Khademhosseini, Tissue adhesive hemostatic microneedle arrays for rapid hemorrhage treatment, Bioact Mater 23 (2023) 314–327, https://doi.org/10.1016/j.bioactmat.2022.08.017.
[18] S. Tan, Y. Qiu, H. Xiong, C. Wang, Y. Chen, W. Wu, Z. Yang, F. Zhao, Mussel-inspired cortical bone-adherent bioactive composite hydrogels promote bone augmentation through sequential regulation of endochondral ossification, Mater. Today Bio. 23 (2023) 100843, https://doi.org/10.1016/j.mtbio.2023.100843.
[19] C. Cai, Z. Chen, Y. Chen, H. Li, Z. Yang, H. Liu, Mechanisms and applications of bioinspired underwater/wet adhesives, J. Polym. Sci. 59 (2021) 2911–2945, https://doi.org/10.1002/pol.20210521.
[20] L. Chen, H.Z. An, R. Haghgooie, A.T. Shank, J.M. Martel, M. Toner, P.S. Doyle, Flexible octopus-shaped hydrogel particles for specific cell capture, Small 12 (2016) 2001–2008, https://doi.org/10.1002/smll.201600163.
[21] S.T. Frey, A.B.M.T. Haque, R. Tutika, E.V. Krotz, C. Lee, C.B. Haverkamp, E. J. Markvicka, M.D. Bartlett, Octopus-inspired adhesive skins for intelligent and rapidly switchable underwater adhesion, Sci. Adv. 8 (2022) eabq1905, https://doi.org/10.1126/sciadv.abq1905.
[22] W. Liu, R. Xie, J. Zhu, J. Wu, J. Hui, X. Zheng, F. Huo, D. Fan, A temperature responsive adhesive hydrogel for fabrication of flexible electronic sensors, npj Flexible Electron 6 (2022) 68, https://doi.org/10.1038/s41528-022-00193-5.
[23] R. Huang, X. Zhang, W. Li, L. Shang, H. Wang, Y. Zhao, Suction cups-inspired adhesive patch with tailorable patterns for versatile wound healing, Adv. Sci. 8 (2021) 2100201, https://doi.org/10.1002/advs.202100201.
[24] Y.C. Chen, H. Yang, Octopus-inspired assembly of nanosucker arrays for dry/wet adhesion, ACS Nano 11 (2017) 5332–5338, https://doi.org/10.1021/acsnano.7b00809.
[25] H. Lee, D.S. Um, Y. Lee, S. Lim, H.J. Kim, H. Ko, Octopus-inspired smart adhesive pads for transfer printing of semiconducting nanomembranes, Adv. Mater. 28 (2016) 7457–7465, https://doi.org/10.1002/adma.201601407.
[26] J. Li, Z. Song, C. Ma, T. Sui, P. Yi, J. Liu, A bioinspired adhesive sucker with both suction and adhesion mechanisms for three-dimensional surfaces, J. Bionic Eng. 19 (2022) 1671–1683, https://doi.org/10.1007/s42235-022-00238-5.
[27] X. Fan, Y. Fang, W. Zhou, L. Yan, Y. Xu, H. Zhu, H. Liu, Mussel foot protein inspired tough tissue-selective underwater adhesive hydrogel, Mater. Horiz. 8 (2021) 997–1007, https://doi.org/10.1039/D0MH01231A.
[28] X. Su, Y. Luo, Z. Tian, Z. Yuan, Y. Han, R. Dong, L. Xu, Y. Feng, X. Liu, J. Huang, Ctenophore-inspired hydrogels for efficient and repeatable underwater specific adhesion to biotic surfaces, Mater. Horiz. 7 (2020) 2651–2661, https://doi.org/10.1039/D0MH01344G.
[29] S.H. Hiew, J.K. Wang, K. Koh, H. Yang, A. Bacha, J. Lin, Y.S. Yip, M.I.G. Vos, L. Chen, R.M. Sobota, N.S. Tan, C.Y. Tay, A. Miserez, Bioinspired short peptide hydrogel for versatile encapsulation and controlled release of growth factor therapeutics, Acta Biomater 136 (2021) 111–123, https://doi.org/10.1016/j.actbio.2021.09.023.
[30] H. Yuk, C.E. Varela, C.S. Nabzdyk, X. Mao, R.F. Padera, E.T. Roche, X. Zhao, Dry double-sided tape for adhesion of wet tissues and devices, Nature 575 (2019) 169–174, https://doi.org/10.1038/s41586-019-1710-5.
[31] J. Yu, Y. Qin, Y. Yang, X. Zhao, Z. Zhang, Q. Zhang, Y. Su, Y. Zhang, Y. Cheng, Robust hydrogel adhesives for emergency rescue and gastric perforation repair, Bioact. Mater. 19 (2023) 703–716, https://doi.org/10.1016/j.bioactmat.2022.05.010.
[32] Y. Yang, Y. Xiao, X. Wu, J. Deng, R. Wei, A. Liu, H. Chai, R. Wang, Microgel-crosslinked thermo-responsive hydrogel actuators with high mechanical properties and rapid response, Macromol. Rapid. Commun. 45 (2024) 2300643, https://doi.org/10.1002/marc.202300643.
[33] P. Sun, H. Zhang, D. Xu, Z. Wang, L. Wang, G. Gao, G. Hossain, J. Wu, R. Wang, J. Fu, Super tough bilayer actuators based on multi-responsive hydrogels crosslinked by functional triblock copolymer micelle macro-crosslinkers, J. Mater. Chem. B. 7 (2019) 2619–2625, https://doi.org/10.1039/C9TB00249A.
[34] F. Chen, G. Lu, H. Yuan, R. Li, J. Nie, Y. Zhao, X. Shu, X. Zhu, Mechanism and regulation of LCST behavior in poly(hydroxypropyl acrylate)-based temperature-sensitive hydrogels, J. Mater. Chem. A. 10 (2022) 18235–18247, https://doi.org/10.1039/D2TA04271A.
[35] T. Kyrey, J. Witte, J. Lutzki, M. Zamponi, S. Wellert, O. Holderer, Mobility of bound water in PNIPAM microgels, Phys. Chem. Chem. Phys. 23 (2021) 14252–14259, https://doi.org/10.1039/D1CP01823J.
[36] H. Takahashi, T. Okano, Thermally-triggered fabrication of cell sheets for tissue engineering and regenerative medicine, Adv. Drug Deliver. Rev. 138 (2019) 276–292, https://doi.org/10.1016/j.addr.2019.01.004.
[37] Q.-T. Pham, Z.-H. Yao, Y.-T. Chang, F.-M. Wang, C.-S. Chern, LCST phase transition kinetics of aqueous poly(N-isopropylacrylamide) solution, J. Taiwan Inst. Chem. Eng. 93 (2018) 63–69, https://doi.org/10.1016/j.jtice.2018.07.045.
[38] X. Xu, K. Shibata, M. Ouchi, Precision syntheses of poly(NIPAM-*alt*-HEMA) and effects of the alternating sequence on thermoresponsive behaviors in water, Polym. Chem. 14 (2023) 55–61, https://doi.org/10.1039/D2PY01196D.
[39] T. Maeda, K. Yamamoto, T. Aoyagi, Importance of bound water in hydration–dehydration behavior of hydroxylated poly(*N*-isopropylacrylamide), J. Colloid Interface Sci. 302 (2006) 467–474, https://doi.org/10.1016/j.jcis.2006.06.047.
[40] X. Chen, H. Yuk, J. Wu, C.S. Nabzdyk, X. Zhao, Instant tough bioadhesive with triggerable benign detachment, Proc. Natl. Acad. Sci. U S A. 117 (2020) 15497–15503, https://doi.org/10.1073/pnas.2006389117.
[41] C.Y. Cui, B. Li, D. Cheng, X.Y. Li, J.L. Chen, Y.T. Chen, X.C. Su, Simultaneous Quantification of Biothiols and Deciphering Diverse GSH Stability in Different Live Cells by ^{19}F-Tag, Anal Chem 94 (2021) 901–908, https://doi.org/10.1021/acs.analchem.1c03673.
[42] X. Wei, J.-Y. Wang, X. Yang, J.-Y. Wu, R. Hong, Y. Liu, J. Gou, J. Hu, K. Li, L. Li, J.-Z. X, Z.-M. Li, Wet adhesion enhancement through citric-acid-regulated supramolecular network, Compos. Part B-Eng. 265 (2023) 110964, https://doi.org/10.1016/j.compositesb.2023.110964.